PCCP

PAPER

View Article Online
View Journal | View Issue

Cite this: *Phys. Chem. Chem. Phys.*, 2019, **21**, 3287

Mapping the dynamics of methanol and xenon co-adsorption in SWNTs by *in situ* continuous-flow hyperpolarized ^{129}Xe NMR†

Shutao Xu, *[a] Xin Li,[b] Cheng Sun,[c] Anmin Zheng,[d] Weiping Zhang,[e] Xiuwen Han,[a] Xianchun Liu[a] and Xinhe Bao *[a]

Received 24th November 2018,
Accepted 15th January 2019

DOI: 10.1039/c8cp07238h

rsc.li/pccp

A comparative study of the adsorption and desorption processes of methanol in two kinds of nanochannels (*i.e.* MCM-41 and SWNTs) is performed by *in situ* continuous-flow laser-hyperpolarized ^{129}Xe NMR. The high sensitivity and short acquisition time of hyperpolarized ^{129}Xe allow for probing the molecular dynamics in a confined geometry under real working conditions. Hyperpolarized ^{129}Xe NMR spectra indicate that the methanol adsorption behavior in nanochannels is determined by the characters of adsorption sites and that the methanol adsorption rate in the nanochannels of SWNTs is faster than in MCM-41. The experimental data shown in this work also indicate that there is a change in gas phase ^{129}Xe NMR signal intensity during the adsorption and desorption of methanol in SWNTs. This may be because there is a strong depolarization of hyperpolarized ^{129}Xe in SWNTs.

Introduction

Molecules adsorbed in confined nanoporous spaces such as nanochannels can display unique properties that differ significantly from those in the bulk.[1–3] Among these nanoscale materials, carbon nanotubes (CNTs), possessing one dimensional nanochannels and atomically smooth surfaces, have extraordinary mechanical strength, electrical conductivity, thermal stability and optical properties.[4–7] To date, a variety of potential applications of CNTs in chemical sensors, energy storage and catalysis have been demonstrated.[8–12] For example, an important application of carbon nanotubes is that they can be used as catalysts or supports in heterogeneous catalysis to enhance the activities and selectivity of the related reactions.[10–12] CNTs have extraordinary electronic properties resulting from the deformed sp2 hybridization electron structure of the graphene walls. Deviation from planarity causes π-electron density to shift from the concave inner to the convex outer surface, leading to an electron potential difference between inside and outside of CNTs.[13–15] Therefore, CNTs provide favorable confined electron environments wherein strong interaction is formed with species that are restricted in the nanochannels of CNTs. This may result in different properties of molecules confined within CNTs from those on the exterior walls of CNTs. For example, *in situ* HRTEM, XRD, Raman spectroscopy and temperature-programmed desorption (TPD) experiments revealed that the reduction of Fe_2O_3 particles inside the channels of CNTs were facilitated distinctly with respect to those sitting on the external surface of the tubes.[11,12] In addition, confinement of a bicomponent RhMn catalyst in CNT channels (RhMn-in) was found to enhance its catalytic activity for syngas conversion to C_2 oxygenates with respect to the outside catalyst (RhMn-out) and the RhMn catalyst in SBA-15 (a silicate-based material with the same channel size).[11,12] The much better catalytic performances of CNTs as supports than SBA-15 are not only attributed to its outstanding electronic properties, but may also be due to its excellent adsorption and diffusion properties.

Many theoretical simulations have shown that molecular adsorption and diffusion inside CNTs play a crucial role in the above applications.[16–19] Adsorption isotherms, infrared (IR) spectroscopy, temperature programmed desorption (TPD) and Raman spectroscopy have been widely used to study the adsorption of the gas molecules in CNTs.[20–27] Compared to these methods, nuclear magnetic resonance (NMR) can provide information about molecular adsorption and interaction between molecules and nanotubes. Sekhaneh *et al.* and Chen *et al.* employed the ^{1}H MAS NMR technique and assigned two proton chemical

[a] *State Key Laboratory of Catalysis, Dalian Institute of Chemical Physics, Chinese Academy of Sciences, 457 Zhongshan Road, Dalian 116023, China. E-mail: xushutao@dicp.ac.cn, xhbao@dicp.ac.cn*
[b] *College of Chemistry and Chemical Engineering, Henan University of Technology, Zhengzhou 450001, China*
[c] *College of Physical Science and Technology, Dalian University, Dalian, China*
[d] *State Key Laboratory of Magnetic Resonance and Atomic and Molecular Physics, Wuhan Center for Magnetic Resonance, Wuhan Institute of Physics and Mathematics, Chinese Academy of Sciences, Wuhan 430071, China*
[e] *State Key Laboratory of Fine Chemicals, School of Chemical Engineering, Dalian University of Technology, Dalian 116024, China*

† Electronic supplementary information (ESI) available. See DOI: 10.1039/c8cp07238h

shift ranges to the water adsorbed inside and outside the nanotubes.[28,29] Our group also previously used ^{13}C MAS NMR to investigate the adsorption of ^{13}C-enriched methanol in multi-walled carbon nanotubes (MWNTs).[30] The results indicate that the endohedral adsorption of methanol in MWNTs is preferential over the exohedral adsorption. The ^{13}C chemical shift of endohedral methanol exhibits a large upfield shift due to the strong spatial diamagnetic shielding effect induced by the delocalized electrons of nanotubes under the influence of an external magnetic field.[30] ^{129}Xe and HP ^{129}Xe NMR spectroscopies have been widely used in the characterization of porous materials, including microporous zeolites, mesoporous silica, polymers, metal–organic-framework (MOF) materials, *etc.* due to the high sensitivity and large range chemical shift of ^{129}Xe.[31–35] It can provide detailed information on the size, shape, and local electronic structure of the pores within their frameworks.

Previously, we proposed a novel approach of *in situ* continuous-flow laser-hyperpolarized (HP) ^{129}Xe MAS NMR to study the adsorption and reaction kinetics in nanocages.[36] In our strategy, laser-hyperpolarized ^{129}Xe was achieved by spin-exchange optical pumping to tremendously enhance the signal intensity by 4 to 5 orders of magnitude compared to conventional ^{129}Xe NMR.[37–39] HP ^{129}Xe was then premixed with an adsorbate outside the NMR probe and made to enter the high-field coil region through an NMR rotor where the sample was located (Fig. S1, ESI†). In this case, it was possible for us to monitor the dynamic process in a confined space at the earliest stage by HP ^{129}Xe NMR spectroscopy, which has much higher sensitivity and shorter acquisition time in the order of a few to tens of seconds per spectrum. In this paper, we apply this technique to investigate the molecular adsorption and desorption processes in SWNTs, and compare them with a silicate-based material, MCM-41. The depolarization of HP ^{129}Xe due to electron–nuclear interaction between SWNTs and HP ^{129}Xe is also studied.

Results and discussion

Methanol adsorption and desorption in MCM-41 nanochannels

In order to better understand the adsorption and desorption behaviors of methanol molecules inside SWNTs, we first performed experiments on methanol in a silicate-based material MCM-41 that had similar pore sizes to the SWNTs (Fig. S2–S4, ESI†). MCM-41 is a silicate compound that has a hexagonal array of uniform one dimensional mesopores with diameters ranging from 2 to 10 nm. We chose MCM-41 with an average diameter of 2 nm to investigate the adsorption and desorption of methanol molecules in its nanochannels; the diameter was comparable to that of the SWNTs we used in the present work. Generally, the dependence of the ^{129}Xe NMR chemical shift δ on a number of different variables for Xe adsorption in porous materials can be summarized by the following expression:

$$\delta = \delta_{ref} + \delta_s + \delta_{Xe\text{–}Xe} + \delta_{SAS} + \delta_E + \delta_M$$

where δ_{ref} is the reference (gaseous xenon at zero pressure, normally set to 0 ppm), δ_s indicates the interaction between xenon and the surface which is always affected by channel size and shape, $\delta_{Xe\text{–}Xe}$ describes the contribution from collisions with other xenon atoms and is related to the concentration of the xenon atom, δ_{SAS} indicates the presence of strong adsorption sites, and δ_E and δ_M represent the presence of electric or magnetic fields that can perturb the ^{129}Xe chemical shift.[40] For the HP ^{129}Xe system, the concentration of gas phase xenon is very low ($\sim$1%) and the contribution of Xe–Xe interactions is rather insignificant at ambient temperature, and the observed ^{129}Xe chemical shift could reflect mainly interactions between xenon atoms and the surface, *i.e.*, the chemical composition of the surface and the geometry of the xenon environment in that particular site. However, at lower temperature, the Xe–Xe interactions in the pores cannot be excluded due to the higher concentration of xenon atoms.[37–39] For a porous material, the HP ^{129}Xe NMR signal can arise from the average chemical shifts weighted by the xenon's dwell time in the various locations. Four possible sample regions for xenon staying have been proposed: the xenon atoms in the overhead gas (reservoir I), xenon in the interparticle space (reservoir II), xenon inside the crystallites within an exchangeable layer surrounding the crystallites (reservoir III), and xenon atoms deep inside the crystal (reservoir IV).[41,42]

Fig. 1a shows the *in situ* HP ^{129}Xe MAS NMR spectra highlighting the evolution of the adsorption and desorption of methanol molecules in MCM-41 nanochannels at -20 °C. The peaks at 0 ppm in the spectra are due to the gas phase xenon (labelled OUT-xenon below). All signals at lower field originated from adsorbed xenon in the MCM-41 nanochannels (labeled IN-xenon). Before the introduction of methanol, the chemical shift of ^{129}Xe in nanochannels is 80 ppm. After methanol is co-injected with the HP xenon into the rotor reactor, the signal of IN-xenon moves to a lower field and the peak intensity of IN-xenon decreases, which can be attributed to methanol adsorption in the nanochannels. In our case, the chemical shifts of HP ^{129}Xe for both MCM-41 and SWNT are much larger than that of gas phase xenon (0 ppm) at room temperature. Therefore, the adsorbed signal at lower field should be ascribed to the xenon atom in reservoir IV due to the spatial confinement. When methanol adsorbed on MCM-41, a much lower field chemical shift of ^{129}Xe was observed. It indicated that methanol was adsorbed in the interior channels (reservoir IV). Finally, after about 60 min, the signal of IN-xenon nearly disappears, which indicates that the adsorption process of methanol reaches a steady state. When methanol gas is switched off, the signal of IN-xenon gradually recovers with time, which indicates that methanol is desorbed from the nanochannels since the adsorbed xenon increases. Therefore, the methanol adsorption and desorption processes may be quantified, to some extent, by the rates of the intensity change of IN-xenon. Fig. 1b highlights the time variation in relative peak intensities of IN-xenon and OUT-xenon. The signals of IN-xenon and OUT-xenon were normalized respectively to the spectra that had the corresponding largest intensities. From Fig. 1b, we observe a two-rate process for both the adsorption and desorption.

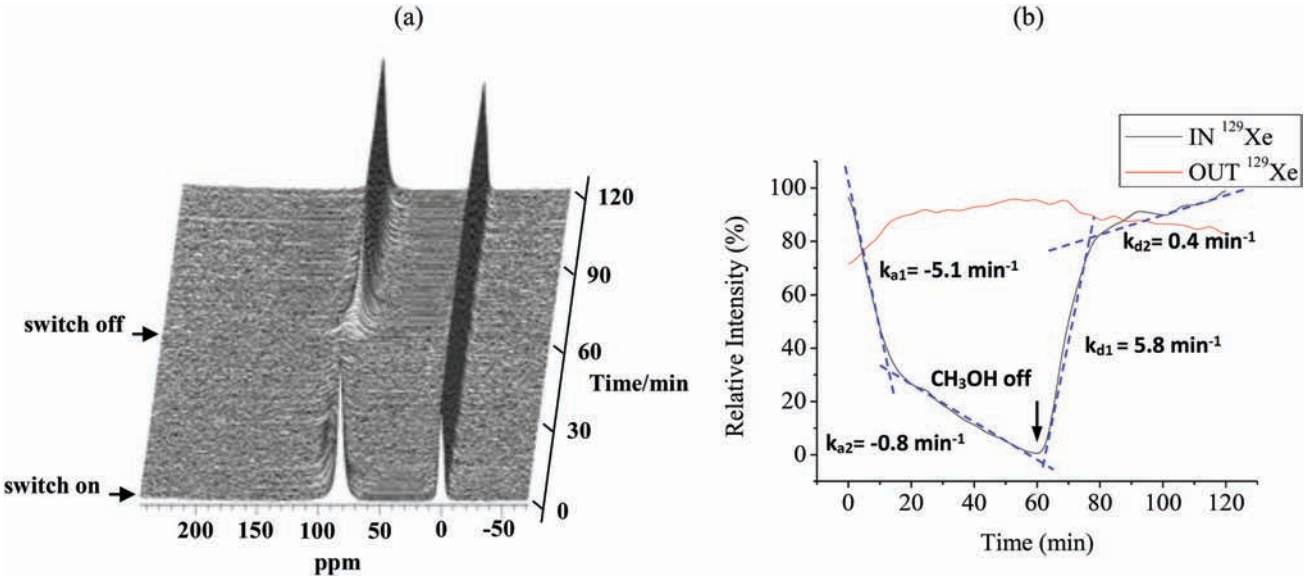

Fig. 1 (a) *In situ* HP ^{129}Xe MAS NMR spectra recorded as a function of time, with a time resolution of 30 s per spectrum during adsorption and desorption of methanol in MCM-41 nanochannels at −20 °C; (b) time variation in relative peak intensities of ^{129}Xe in nanochannels and in the gas phase. The solid lines represent normalized experimental data, described in the text.

Based on this observation, the adsorption and desorption processes are proposed below:

$$CH_3OH(g) + [MCM\text{-}41]_{empty} \xrightarrow{k_{a1}} CH_3OH@[MCM\text{-}41] \quad (1)$$

$$CH_3OH@[MCM\text{-}41] + (n-1)CH_3OH(g) \xrightarrow{k_{a2}} (CH_3OH)_n@[MCM\text{-}41] \quad (2)$$

$$(CH_3OH)_n@[MCM\text{-}41] \xrightarrow{k_{d1}} CH_3OH@[MCM\text{-}41] + (n-1)CH_3OH(g) \quad (3)$$

$$CH_3OH@[MCM\text{-}41] \xrightarrow{k_{d2}} CH_3OH(g) + [MCM\text{-}41]_{empty} \quad (4)$$

First, there is an initial period of rapid adsorption, which is attributed to the methanol molecules being adsorbed on ready silanol groups of MCM-41 *via* hydrogen bonds; this is shown by eqn (1) with a fast rate of k_{a1}. Then, more and more methanol molecules are adsorbed in the nanochannels of MCM-41 with a slower rate k_{a2}. In this period, shown by eqn (2), methanol molecules aggregate in the form of clusters or are adsorbed as multilayers by van der Waals force. An opposite two-step process is observed when the methanol gas is off. As indicated in eqn (3) and (4), the initial desorption of methanol (eqn (3)) is faster than the one later (eqn (4)), this is because the aggregated methanol molecules have weaker interaction with MCM-41 nanochannels and hence are more easily removed by xenon gas with a fast rate k_{d1}. The adsorbed methanol molecules are subsequently desorbed with a slower rate k_{d2}, due to its stronger interaction *via* hydrogen bonds with MCM-41. By fitting the data of IN-xenon in Fig. 1b to linear equations, the two kinds of adsorption rate for methanol adsorption in MCM-41 nanochannels are determined to be $k_{a1} = -5.1$ min^{-1} and $k_{a2} = -0.8$ min^{-1} and the desorption rates of methanol are determined to be $k_{d1} = 5.8$ min^{-1} and $k_{d2} = 0.4$ min^{-1}. Our results are consistent with the work of Xu *et al.* wherein they used the ^{1}H MAS NMR method to investigate water molecules adsorbed on MCM-41, and also found a two-rate process for water adsorption in MCM-41.[43] In addition, we also investigated the situation at 0 and 20 °C (Fig. S5 and S6, ESI†). The adsorption and desorption processes will be accelerated when the temperatures increase which makes it difficult to distinguish the two-step adsorption or desorption processes at 20 °C.

Methanol adsorption and desorption in SWNT nanochannels

Fig. 2a shows the *in situ* HP ^{129}Xe MAS NMR spectra recording the time evolution of the adsorption and desorption of methanol molecules in SWNT nanochannels at −20 °C. The peaks at 0 ppm in the ^{129}Xe NMR spectra are due to OUT-xenon. All signals at lower field originated from the IN-xenon in the SWNT nanochannels because the SWNTs were not densely packed. It is observed that before the introduction of methanol gas, the chemical shift of ^{129}Xe in the empty nanochannels is approximately 71 ppm. The chemical shift slightly moves to high field and the signal intensity rapidly decreases when switching on methanol gas. This is due to the fast adsorption of methanol molecules in SWNTs, described in eqn (5) as follows:

$$CH_3OH(g) + [SWNTs]_{empty} \xrightarrow{k_a} CH_3OH@[SWNTs] \quad (5)$$

After about 3 min, the adsorbed peak remains unchanged indicating that the adsorption of methanol reaches a steady state. Then, the adsorbed peak intensity increases to the original value after switching off methanol gas, indicating a desorption process of methanol, shown by eqn (6):

$$CH_3OH@[SWNTs] \xrightarrow{k_d} CH_3OH(g) + [SWNTs]_{empty} \quad (6)$$

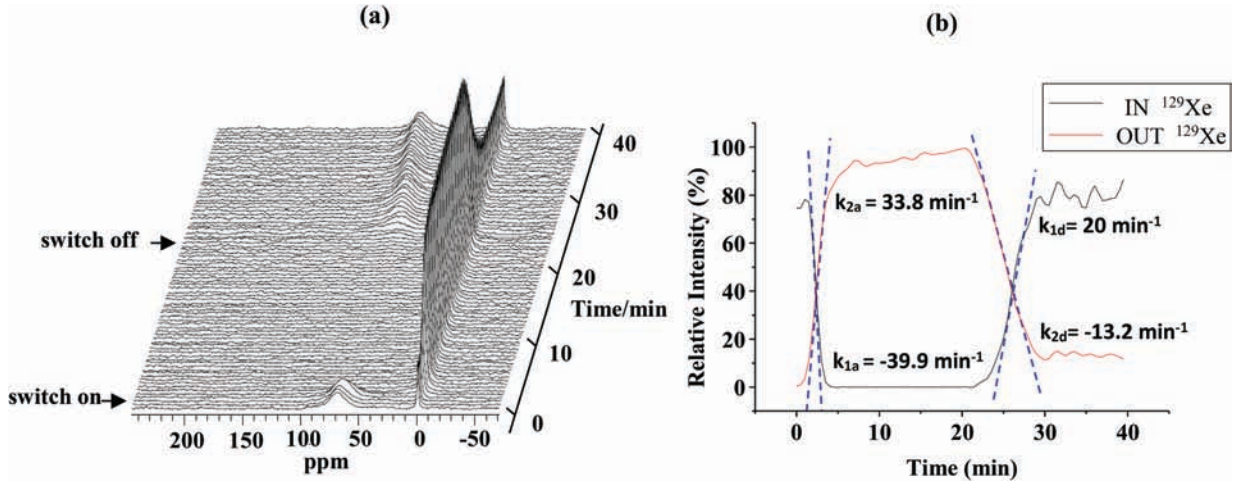

Fig. 2 (a) *In situ* HP ^{129}Xe MAS NMR spectra recorded as a function of time, with a time resolution of 30 s per spectrum during adsorption and desorption of methanol in SWNT nanochannels at −20 °C; (b) time variation in relative peak intensities of ^{129}Xe in nanochannels and the gas phase. The solid lines represent normalized experimental data, described in the text, and the dashed lines are the best fits to the data of ^{129}Xe in nanochannels.

There are two possible adsorption sites for methanol in SWNTs. One is the interior nanochannel (reservoir IV) and the other is the position near the nanotube openings (reservoir III). The relative peak intensities of IN-xenon and OUT-xenon are shown in Fig. 2b, normalized in the same fashion mentioned above as that of MCM-41. From the decay rates of the IN-xenon signal intensities shown in Fig. 1b and 2b, the adsorption rate for methanol in SWNTs, $k_{1a} = -39.9$ min^{-1}, is found to be faster than both adsorption processes in MCM-41, that is, 8 times faster than process (1) in MCM-41 and 50 times faster than process (2) in MCM-41. Similar features were also observed at 0 and 20 °C (Fig. S7 and S8, ESI†). Referring to Fig. S8 and S9 (ESI†), the equilibrium times for methanol adsorption and desorption reduce slightly with increasing temperature. At all the temperatures studied, the adsorption and desorption rates of methanol in SWNTs are faster than that in MCM-41 at a given temperature. According to the MS results (Fig. S9, ESI†), the adsorption and desorption rates of methanol in SWNTs are obtained by fitting the curve of methanol concentration variation with time to linear equations, that is, $v_{a1} = 4.2 \times 10^{-12}$ s^{-1} and $v_{d1} = -4.4 \times 10^{-12}$ s^{-1}, respectively. And for MCM-41, the adsorption and desorption rates are $v_{a2} = 1.4 \times 10^{-12}$ s^{-1} and $v_{d2} = -1.7 \times 10^{-12}$ s^{-1}, respectively. Therefore, the adsorption or desorption rate for methanol in SWNTs is about 3 times faster than in MCM-41, which is consistent with the results of *in situ* HP ^{129}Xe NMR spectra. Unlike MCM-41, there is only one adsorption or desorption process for methanol in SWNTs. This may be due to the lower amounts of hydroxyl species and the faster adsorption rate of methanol in SWNTs. The weaker interaction and adsorption site near the nanotube openings should contribute to the fast adsorption rate of methanol in SWNTs. For classical uptake experiments of gas diffusion in CNTs,[44,45] the measured gas flow exceeds the predictions of the Knudsen diffusion model by more than an order of magnitude. Our *in situ* HP ^{129}Xe NMR method gives the comparative results of methanol adsorption rates in the nanochannels of SWNTs has the faster rate by about 8 and 50 times than that in MCM-41 for the adsorption process (1) and (2), respectively. However, the principal difference between these two methods is that classical uptake methods give the macroscopic transportation rate for methanol, including methanol in the nanochannels and gas phase, while *in situ* HP ^{129}Xe NMR methods give the adsorption or desorption rate for methanol only in the nanochannels.

It is noteworthy that the ^{129}Xe NMR chemical shift trend in SWNTs (*i.e.* upfield shift upon switching on methanol in Fig. 2a) is opposite to that observed in MCM-41 when methanol is co-adsorbed in the nanochannels (*i.e.* downfield shift upon switching on methanol in Fig. 1a). As we all know, the ^{129}Xe NMR chemical shift could be affected by many factors that have been shown above. In the system we studied, the adsorption of methanol would affect the concentration of xenon in the nanochannels, thus the concentrations of Xe and methanol and the interaction between them would be the effect factors to change the ^{129}Xe chemical shift. Therefore, we studied the changes in the ^{129}Xe NMR chemical shift in both the SWNTs and silica material VFI zeolites with a similar channel size after methanol co-adsorption by theoretical simulations, and Fig. 3 shows the simulated results. It can be seen, in the case of only xenon in nanochannels, that the amount of adsorbed Xe in SWNTs (*i.e.* above 100 per cell in Fig. 3a) is greater than that in zeolites (*i.e.* less than 70 per cell in Fig. 3b), which shows the enrichment effect of SWNTs for their adsorbates. The same phenomena of H_2 and CO enriched by SWNTs have also been found by Guan *et al.*[46] After co-adsorption of methanol, the amount of Xe in CNTs decreases greatly under the low pressure conditions that mimic the experiments (Fig. 3a), while it does not change obviously in zeolites (see Fig. 3b). It may be due to the large space left here in zeolites as the adsorption amount of Xe is small. The higher the pressure of methanol is, the lower the amount of adsorbed Xe in the nanochannels of SWNTs is. In order to compare the influence of the Xe–Xe and Xe–CH_3OH interactions on ^{129}Xe NMR chemical shifts, we calculated the

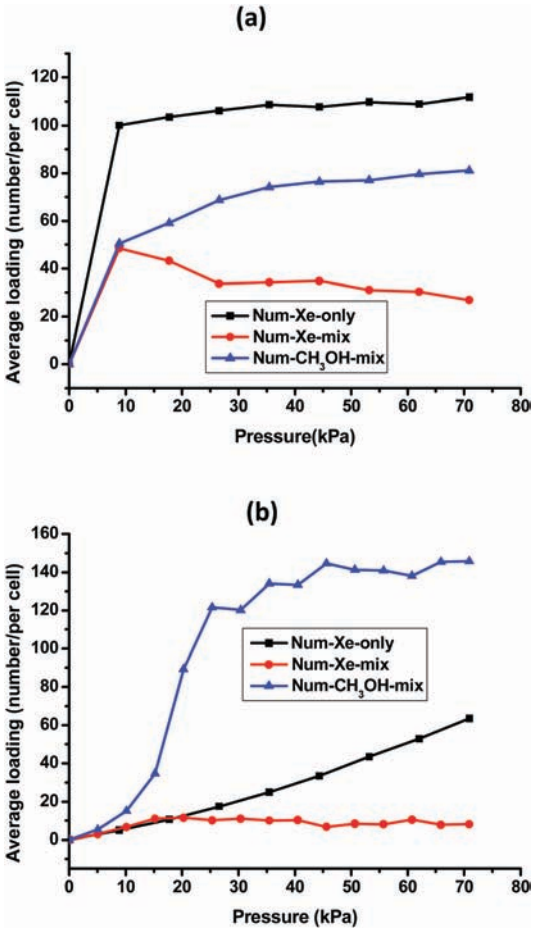

Fig. 3 Isotherms of Xe and CH_3OH co-adsorbed in SWNT (10,10) (a) and Si-VFI zeolite (b). Num-Xe-only denotes the number of Xe adsorbed in the nanochannels for pure Xe status, and Num-Xe-mix and Num-CH_3OH-mix denote the number of Xe and CH_3OH, respectively, in the nanochannels for Xe and CH_3OH mixture status.

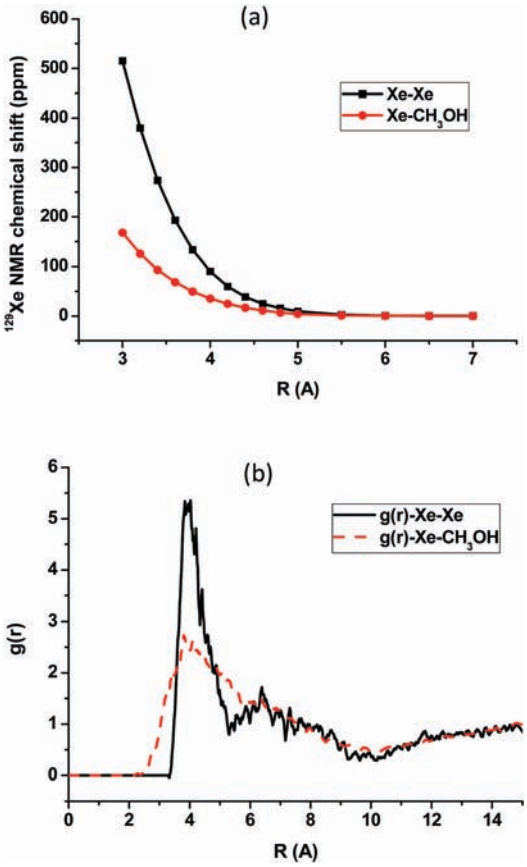

Fig. 4 (a) The calculated ^{129}Xe NMR chemical shifts of Xe–Xe or Xe–CH_3OH with various molecular distances. (b) Radius distribution functions (RDF) between Xe–Xe and Xe–CH_3OH in SWNT (10,10) at a pressure of 0.1 atm by the Grand Canonical Monte Carlo (GCMC) method. The solid line denotes the RDF of Xe–Xe and the dashed line denotes the RDF of Xe–CH_3OH. The selected pressure of 0.1 atm is based on the experimental partial pressure of Xe and CH_3OH of about 0.1 atm.

^{129}Xe NMR chemical shifts in both Xe–Xe and Xe–CH_3OH systems (see Fig. 4a). It is found that the contribution of Xe–Xe interaction is greater than that of Xe–CH_3OH at the same molecular distance. And the radius distribution function (RDF) of Xe–Xe or Xe–CH_3OH in SWNTs (Fig. 4b) shows that the most probable distributed distances of Xe–Xe and Xe–CH_3OH are both 4 Å. So the contribution to ^{129}Xe NMR chemical shifts of Xe–Xe interaction is greater than that of Xe–CH_3OH interaction according to Fig. 4a. As we discussed above, there exists a great increase of Xe–CH_3OH interaction with a nearly unchanged Xe–Xe interaction in the zeolite system, so the overall ^{129}Xe NMR chemical shift would downshift with methanol co-adsorption since the net interaction on ^{129}Xe by its surrounding molecules increases. However, in CNTs, after methanol adsorption, the interaction of Xe–methanol increases with the notable weakening of the Xe–Xe interaction. From Fig. 4, we know that the latter has an even stronger influence on the total ^{129}Xe NMR chemical shift. So an opposite phenomenon to zeolites can be found in the CNT system with the ^{129}Xe NMR chemical shift shifting to upfield as the net interaction on ^{129}Xe decreases.

Interaction of HP ^{129}Xe with nanochannels

Referring to Fig. 2b, another interesting observation is the obvious change in the OUT ^{129}Xe signal in SWNTs during the whole process. When switching on methanol gas, the intensity of OUT ^{129}Xe increases with time. After switching off methanol gas, the intensity of OUT ^{129}Xe decreases to nearly the original value. This observation is attributed to the depolarization of HP ^{129}Xe in nanochannels, as demonstrated in Fig. 5. The observable OUT ^{129}Xe NMR signal is dominated by the residual HP ^{129}Xe signal which may be weakened by the interaction between HP ^{129}Xe and the surfaces of nanochannels. Because SWNTs have non-localized electrons, and hence are treated as paramagnetic materials, HP ^{129}Xe inside the nanochannels is easily depolarized due to its interaction with the electrons of SWNTs. Therefore, the HP ^{129}Xe diffused out from the nanochannels contributes less to the OUT ^{129}Xe NMR signal compared to that outside the nanochannels. Referring to Fig. 5a, when there are no methanol molecules, the xenon molecules are free to diffuse through the nanochannels in SWNTs. However, the through-channel diffusion pathway is blocked to some extent once methanol gas is introduced, as indicated in Fig. 5b. The overall OUT-xenon signal is greater in

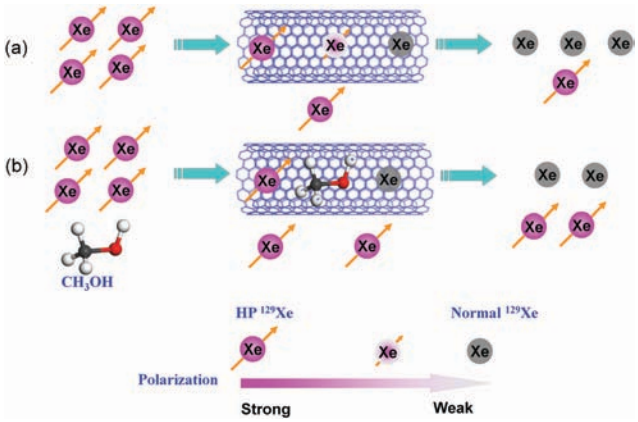

Fig. 5 The depolarization processes of hyperpolarized ^{129}Xe (a) without and (b) with methanol in SWNTs. The polarization is indicated by both the arrow size on the circle and its color, which is shown by the color bar at the bottom of the figure.

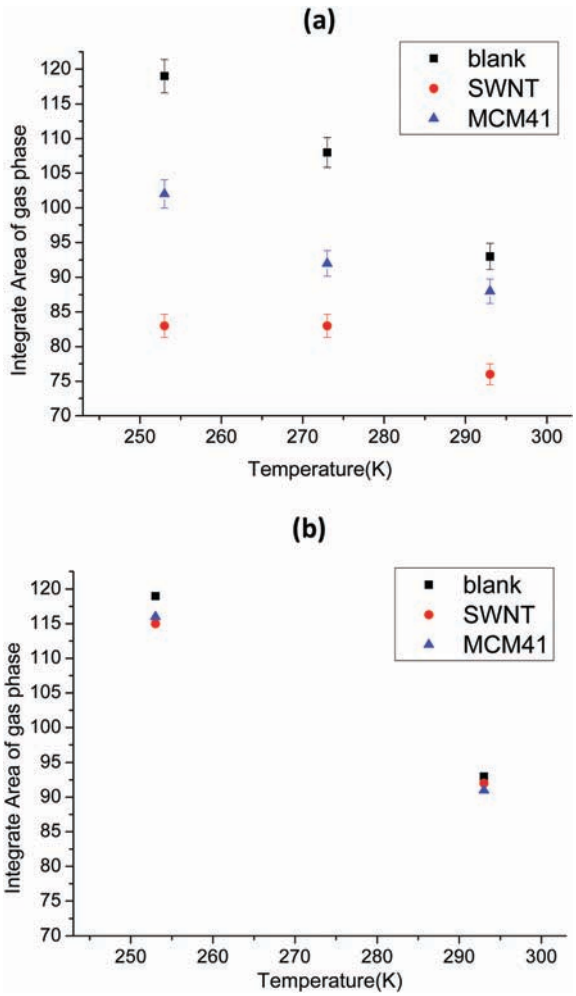

Fig. 6 Comparison of HP ^{129}Xe NMR intensities in the gas phase of different samples at various temperatures: (a) only injection of HP ^{129}Xe in the steady state; (b) co-injection of methanol and HP ^{129}Xe in the steady state. The blank experiment was performed in the same NMR tube which had 10 mg silylated glass wool, and most of the HP ^{129}Xe atoms retained their polarization during the whole experimental process.

the case of Fig. 5b because more HP ^{129}Xe molecules remained outside the nanochannels. The above mechanism is further supported by Fig. 6 wherein the OUT ^{129}Xe NMR signal is plotted (a) before and (b) after methanol gas is introduced. From Fig. 6a, it is clear that at all temperatures studied, for both SWNTs and MCM-41, the ^{129}Xe intensity reduces compared to that in a blank experiment, while the intensity remains almost the same once methanol gas is introduced, as shown in Fig. 6b. The blank experiment performed here gives a referenced maximum value of the OUT ^{129}Xe NMR intensity. The experimental results indicate that the HP ^{129}Xe molecules that diffuse through the nanochannels are easily depolarized. It is also revealed that the depolarization effect in MCM-41 is observed to be smaller than that in SWNTs. This is because MCM-41 has no mobile electrons, and therefore has little paramagnetic electron–nuclear spin interaction. This smaller depolarization effect in MCM-41 is also consistent with the smaller variation observed for the OUT ^{129}Xe signal in Fig. 1b. The adsorption rate K_{2a} derived from OUT ^{129}Xe in Fig. 2b was found to be comparable with K_{1a} derived from IN-^{129}Xe. The ^{129}Xe NMR signal intensity of OUT ^{129}Xe was influenced by the depolarization effect in SWNTs. Thus K_{2a} may reflect the rate of the depolarization effect and it is related to the adsorption rate of methanol.

Conclusions

A novel approach of *in situ* HP ^{129}Xe NMR has been applied to investigate the adsorption and desorption processes of methanol molecules in the nanochannels of SWNTs and MCM-41. Compared with the silica material MCM-41, the rate of methanol adsorption or desorption in SWNT nanochannels has been measured to be faster than that in MCM-41. For MCM-41, a two-rate process has been observed during the adsorption and desorption processes, corresponding to hydrogen bond controlling step and van der Waals force controlling step respectively. However, for SWNTs, only one-rate process has been observed due to the lower amounts of hydroxyl species and the faster adsorption or desorption rate. Theoretical calculations show that the enrichment of Xe occurs in the nanochannels of SWNTs, which results in the opposite trend in the SWNT system with the ^{129}Xe NMR chemical shift shifting to upfield compared with silica material. For SWNTs, the exceptional phenomenon of the gas phase ^{129}Xe signal changes when injection of methanol gas indicates a strong depolarization effect on HP ^{129}Xe caused by the interaction of its nuclear spin with non-localized electrons of SWNTs.

Conflicts of interest

There are no conflicts to declare.

Acknowledgements

We gratefully thank Prof. Kaili Jiang from Tsinghua University for kindly providing the SWNT samples. We thank Prof. Yining Huang from the University of Western Ontario, Prof. Jean-paul

Amoureux from Lille-1 University and Prof. Bingwen Hu from East China Normal University for fruitful discussions. We are grateful for the financial support from the National Natural Science Foundation of China (No. 91545104 and 21473182) and the Youth Innovation Promotion Association of the Chinese Academy of Sciences (2014165).

Notes and references

1 M. Beiner, G. T. Rengarajan, S. Pankaj, D. Enke and M. Steinhart, *Nano Lett.*, 2007, **7**, 1381–1385.
2 J. Ha, J. H. Wolf, M. A. HillmyerA and M. D. Ward, *J. Am. Chem. Soc.*, 2004, **126**, 3382–3383.
3 K. Matsuda, T. Hibi, H. Kadowaki, H. Kataura and Y. Maniwa, *Phys. Rev. B: Condens. Matter Mater. Phys.*, 2006, **74**, 073415.
4 S. Iijima, *Nature*, 1991, **354**, 56–58.
5 H. J. Dai, J. H. Hafner, A. G. Rinzler, D. T. Colbert and R. E. Smalley, *Nature*, 1996, **384**, 147–150.
6 M. Meyyappan, *Carbon Nanotubes Science and Applications*, CRC Press LLC, 2005.
7 R. D. Saito, G. Dresselhaus and M. S. Dresselhaus, *Physical Properties of Carbon Nanotubes*, Imperial College Press, London, 1998.
8 R. H. Baughman, A. A. Zakhidov and W. A. De Heer, *Science*, 2002, **297**, 787–792.
9 M. Endo, M. S. Strano and P. M. Ajayan, *Top. Appl. Phys.*, 2008, **111**, 13–61.
10 J. M. Planeix, N. Coustel, B. Coq, V. Brotons, P. S. Kumbhar, R. Dutartre, P. Geneste, P. Bernier and P. M. Ajayan, *J. Am. Chem. Soc.*, 1994, **116**, 7935–7936.
11 X. L. Pan and X. H. Bao, *Chem. Commun.*, 2008, 6271–6281.
12 X. L. Pan and X. H. Bao, *Acc. Chem. Res.*, 2011, **8**, 553–562.
13 R. C. Haddon, *Science*, 1993, **261**, 1545–1550.
14 D. Ugarte, A. Chatelain and W. A. de Heer, *Science*, 1996, **274**, 1897–1899.
15 B. Shan and K. Cho, *Phys. Rev. B: Condens. Matter Mater. Phys.*, 2006, **73**, 081401.
16 G. Hummer, J. C. Rasaiah and J. P. Noworyta, *Nature*, 2001, **414**, 188–190.
17 A. Skoulidas, D. M. Ackerman, J. K. Johnson and D. S. Sholl, *Phys. Rev. Lett.*, 2002, **89**, 185901.
18 S. Joseph and N. R. Aluru, *Nano Lett.*, 2008, **8**, 452–458.
19 W. L. Shen and X. Li, *RSC Adv.*, 2016, **6**, 91295–91300.
20 D. S. Rawat, L. Heroux, V. Krungleviciute and A. D. Migone, *Langmuir*, 2006, **22**, 234–238.
21 A. Fujiwara, K. Ishii, H. Suematsu, H. Kataura, Y. Maniwa, S. Suzuki and Y. Achiba, *Chem. Phys. Lett.*, 2001, **336**, 205–211.
22 O. Byl, P. Kondratyuk, S. T. Forth, S. A. FitzGerald, L. Chen, J. K. Johnson and J. T. Yates, *J. Am. Chem. Soc.*, 2003, **125**, 5889–5896.
23 D. V. Kazachkin, Y. Nishimura, H. A. Witek, S. Irle and E. Borguet, *J. Am. Chem. Soc.*, 2011, **133**, 8191–8198.
24 A. Kuznetsova, J. T. Yates, J. Liu and R. E. Smalley, *J. Chem. Phys.*, 2000, **112**, 9590–9598.
25 U. Burghaus, D. Bye, K. Cosert, J. Goering, A. Guerard, E. Kadossov, E. Lee, Y. Nadoyama, N. Richter, E. Schaefer, J. Smith, D. Ulness and B. Wymore, *Chem. Phys. Lett.*, 2007, **442**, 344–347.
26 C. Matranga, B. Bockrath, N. Chopra, B. J. Hinds and R. Andrews, *Langmuir*, 2006, **22**, 1235–1240.
27 D. Nishide, T. Wakabayashi, T. Sugai, R. Kitaura, H. Kataura, Y. Achiba and H. Shinohara, *J. Phys. Chem. C*, 2007, **111**, 5178–5183.
28 W. Sekhaneh, M. Kotecha, U. Dettlaff-Weglikowska and W. S. Veeman, *Chem. Phys. Lett.*, 2006, **428**, 143–147.
29 Q. Chen, J. L. Herberg, G. Mogilevsky, H. J. Wang, M. Stadermann, J. K. Holt and Y. Wu, *Nano Lett.*, 2008, **8**, 1902–1905.
30 X. Liu, X. L. Pan, W. L. Shen, P. J. Ren, X. W. Han and X. H. Bao, *J. Phys. Chem. C*, 2012, **116**, 7803–7809.
31 P. Sozzani, S. Bracco and A. Comotti, in *Hyperpolarized Xenon-129 Magnetic Resonance: Concepts, Production, Techniques and Applications*, ed. T. Meersmann and E. Brunner, Royal Society of Chemistry, Cambridge, 2015, pp. 164–184.
32 P. Sozzani, S. Bracco, A. Comotti, M. Mauri, R. Simonutti and P. Valsesia, *Chem. Commun.*, 2006, 1921–1923.
33 A. Comotti, S. Bracco, P. Valsesia, L. Ferretti and P. Sozzani, *J. Am. Chem. Soc.*, 2007, **129**, 8566–8576.
34 A. Comotti, S. Bracco, P. Sozzani, S. Horike, R. Matsuda, J. Chen, M. Takata, Y. Kubota and S. Kitagawa, *J. Am. Chem. Soc.*, 2008, **130**, 13664–13672.
35 S. Pawsey, I. Moudrakovski, J. Ripmeester, L. Q. Wang, G. J. Exarhos, J. L. C. Rowsell and O. M. Yaghi, *J. Phys. Chem. C*, 2007, **111**, 6060–6067.
36 S. T. Xu, W. P. Zhang, X. C. Liu, X. W. Han and X. H. Bao, *J. Am. Chem. Soc.*, 2009, **131**, 13722–13727.
37 W. Happer, E. Miron, S. Schaefer, D. Schreiber, W. A. Vanwijngaarden and X. Zeng, *Phys. Rev. A: At., Mol., Opt. Phys.*, 1984, **29**, 3092–3110.
38 D. Raftery, H. Long, T. Meersmann, P. J. Grandinetti, L. Reven and A. Pines, *Phys. Rev. Lett.*, 1991, **66**, 584–587.
39 D. Raftery, E. MacNamara, G. Fisher, C. V. Rice and J. Smith, *J. Am. Chem. Soc.*, 1997, **119**, 8746–8747.
40 J. L. Bonardet, J. Fraissard, A. Gédéon and M. A. Springuel-Huet, *Catal. Rev.*, 1999, **41**, 115–225.
41 C. J. Jameson, A. K. Jameson, R. E. Gerald and H. M. Lim, *J. Phys. Chem. B*, 1997, **101**, 8418–8437.
42 J. M. Kneller, R. J. Soto, S. E. Surber, J. F. Colomer, A. Fonseca, J. B. Nagy, G. Van Tendeloo and T. Pietraβ, *J. Am. Chem. Soc.*, 2000, **122**, 10591–10597.
43 M. C. Xu, K. D. M. Harris and J. M. Thomas, *J. Am. Chem. Soc.*, 2008, **130**, 5880–5882.
44 B. J. Hinds, N. Chopra, T. Rantell, R. Andrews, V. Gavalas and L. G. Bachas, *Science*, 2004, **303**, 62–65.
45 J. K. Holt, H. G. Park, Y. M. Wang, M. Stadermann, A. B. Artyukhin, C. P. Grigoropoulos, A. Noy and O. Bakajin, *Science*, 2006, **312**, 1034–1037.
46 J. Guan, X. L. Pan, X. Liu and X. H. Bao, *J. Phys. Chem. C*, 2009, **113**, 21687–21692.